ELSEVIER

# A study of low level vibrations as a power source for wireless sensor nodes

Shad Roundy*, Paul K. Wright, Jan Rabaey

*University of California, Berkeley, 2111 Etcheverry Hall, Berkeley, CA 94720, USA*

## Abstract

Advances in low power VLSI design, along with the potentially low duty cycle of wireless sensor nodes open up the possibility of powering small wireless computing devices from scavenged ambient power. A broad review of potential power scavenging technologies and conventional energy sources is first presented. Low-level vibrations occurring in common household and office environments as a potential power source are studied in depth. The goal of this paper is not to suggest that the conversion of vibrations is the best or most versatile method to scavenge ambient power, but to study its potential as a viable power source for applications where vibrations are present. Different conversion mechanisms are investigated and evaluated leading to specific optimized designs for both capacitive MicroElectroMechanical Systems (MEMS) and piezoelectric converters. Simulations show that the potential power density from piezoelectric conversion is significantly higher. Experiments using an off-the-shelf PZT piezoelectric bimorph verify the accuracy of the models for piezoelectric converters. A power density of 70 $\mu$W/cm$^3$ has been demonstrated with the PZT bimorph. Simulations show that an optimized design would be capable of 250 $\mu$W/cm$^3$ from a vibration source with an acceleration amplitude of 2.5 m/s$^2$ at 120 Hz.
© 2002 Elsevier Science B.V.. All rights reserved.

*Keywords:* Energy scavenging; Vibration to electricity conversion; Self powered wireless sensing

## 1. Introduction

The past few years have seen an increasing focus in the research community on small wireless electronic devices. The vision of ubiquitous wireless sensor networks has considerable potential in areas ranging from building monitoring and environment control to military applications. Advances in low power Very Large Scale Integration (VLSI) design [1,2] along with the low duty cycles of wireless sensors have reduced power requirements to the range of tens to hundreds of microwatts. Such low power dissipation opens up the possibility of powering the sensor nodes by scavenging ambient energy from the environment, eliminating the need for batteries and extending the lifetime indefinitely. (The term 'node', or 'sensor node' will be used here to refer to a single physical device consisting of sensors, a transceiver, and supporting electronics, which is connected to a larger wireless network.) This paper will briefly survey a variety of potential ambient power sources and compare them with fixed energy sources (i.e. batteries), following which an in depth study of the potential of converting ambient vibrations to electrical energy will be presented. A comparison of conversion mechanisms and specific designs for capacitive MicroElectroMechancialSystems (MEMS) and piezoelectric generators will also be discussed. Experiments with prototype devices verify the models upon which the designs are based.

## 2. Survey of power sources

The results of a broad survey of potential energy sources for wireless sensor nodes, both fixed energy sources such as batteries and power scavenging sources, are shown in Table 1. The data are taken from a combination of published studies, theory, and experiments carried out by the authors. Where applicable, references are listed. The top portion of the table shows sources that have a fixed level of power generation. Therefore, the lifetime is potentially infinite. The bottom portion of the table shows sources that contain a fixed amount of energy, and therefore the average power generation is a function of lifetime. All power values are normalized to a device size of 1 cm$^3$. It is assumed that if

---

* Corresponding author. Tel.: +1-510-643-6546; fax: +1-510-643-6547.
*E-mail addresses:* shadr@kingkong.me.berkeley.edu (S. Roundy), pwright@robocop.berkeley.edu (P.K. Wright), jan@eecs.berkeley.edu (J. Rabaey).

Table 1
Comparison of power scavenging and energy sources. The top part of the table contains source with a fixed level of power generation; the bottom part of the table contains sources with a fixed amount of energy storage

| | Power density ($\mu$W/cm$^3$) one year lifetime | Power density ($\mu$W/cm$^3$) 10 year lifetime | References (where applicable) |
|---|---|---|---|
| Solar (outdoors) | 15,000—Direct sun, 150—Cloudy day | 15,000—Direct sun, 150—Cloudy day | |
| Solar (indoors) | 6—Office desk | 6—Office desk | |
| Vibrations (piezoelectric conversion) | 250 | 250 | |
| Vibrations (electrostatic conversion) | 50 | 50 | |
| Acoustic noise | 0.003 at 75 dB, 0.96 at 100 dB | 0.003 at 75 dB, 0.96 at 100 dB | |
| Temperature gradient | 15 at 10 °C gradient | 15 at 10 °C gradient | [3] |
| Shoe inserts | 330 | 330 | [4,5] |
| Batteries (non-rechargeable lithium) | 45 | 3.5 | |
| Batteries (rechargeable lithium) | 7 | 0 | |
| Hydrocarbon fuel (micro heat engine) | 333 | 33 | [6] |
| Fuel cells (methanol) | 280 | 28 | |

the entire device size is 1 cm$^3$, then approximately 0.5 cm$^3$ will be available for the power system. Therefore, the values in Table 1 (and throughout the rest of the paper) are based on 0.5 cm$^3$ for the power generating, or storage, device.

The data show that for short lifetimes, batteries are a reasonable solution. However, another solution is required for long lifetimes. Solar cells offer excellent power density in direct sunlight. However, in dim office lighting, or areas with no light, they are inadequate. Power scavenged from thermal gradients is also substantial enough to be of interest if the necessary thermal gradients are available. It is, however, difficult to find greater than a 10 °C thermal gradient in a volume of 1 cm$^3$. As Starner [4] has documented, there is ample power to scavenge from the human body. Fuel cells represent a potentially large improvement over batteries as an energy reservoir. Research to miniaturize fuel cells is currently underway [7] and is very promising. Miniaturized fuel cells could extend the lifetime of a node up to several times that of a battery powered node. However, this is still a fixed energy source, and so would either require re-fueling, or would have a limited lifetime. It should be noted that while the energy density of hydrocarbon fuels used in micro heat engines is very high, the output power of these devices is too high (on the order of 1–10 W) to be of practical use for low power wireless sensor nodes [6]. Furthermore, once started, they are not easily turned off. Their use would therefore

necessitate a large energy storage reservoir to allow for lower power operation over a longer lifetime, thus negating their advantage. As a final note, Table 1 is by no means comprehensive. Many other potential power sources were evaluated, and only those that seemed most applicable have been reported.

As the potential power available from the conversion of mechanical vibrations is abundant enough to be of use, and because this area is largely unexplored, a further study of this subject has been undertaken. A more careful comparison of vibration conversion to solar power and battery power (the most common alternatives) is shown in Fig. 1. The darkened boxes represent the range of solar power (indoors to direct sunlight) and vibration based power generation. If the projected lifetime of the sensor node is only a few years, then batteries provide the easiest and most versatile power source. If adequate light energy is available in the environment in which the node will operate, solar cells offer an attractive solution. However, if the projected lifetime is more than a few years, and sufficient light energy is not available, vibration conversion is an alternative. Low-level mechanical vibrations are available in many environments, and therefore have a potentially wider application domain than some of the sources listed in Table 1. Furthermore, if a hybrid solution consisting of both solar and vibration based power generation were pursued, the application domain would be even greater. The goal of this
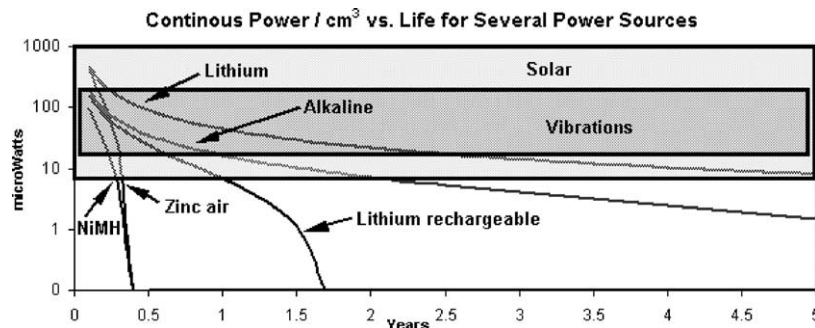


Fig. 1. Comparison of power from vibrations, solar, and various battery chemistries.

**Microwave Casing**

**Windows Next to a Busy Street**

Displacement vs. Freq. - microwave oven

Displacement vs. Freq. - windows

Acceleration vs. Freq. - microwave oven

Acceleration vs. Freq. - windows
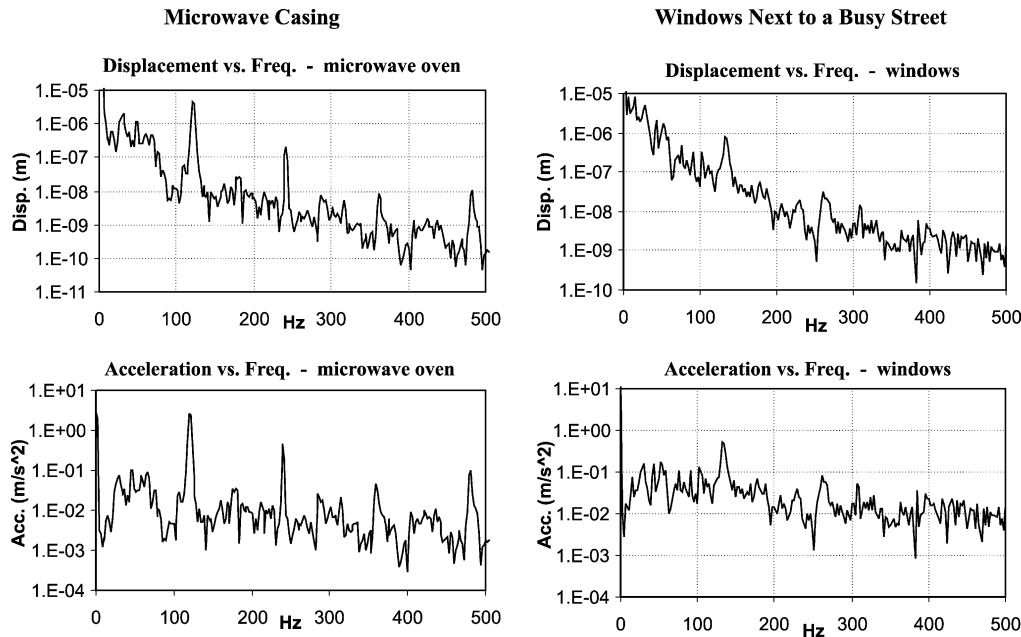
Fig. 2. Vibration spectra for a microwave oven and office windows next to a busy street.

paper is not to suggest that vibration based power sources are the best energy scavenging solution, but to study their potential in applications where vibrations are present.

## 3. Sources of vibration

A variety of commonly occurring vibrations have been measured by the authors in order to investigate the nature of vibrations available. Most of the vibrations measured were from commonly occurring sources, and thus might be classified as 'low level' vibrations. Low-level vibrations were targeted, rather than more energetic vibrations that might be found on large industrial equipment for example, because of the wide range of applications in which they could be used for power generation. Fig. 2 shows the frequency spectrum for two vibration sources: a small microwave oven and large office windows next to a busy street.

The top graph shows displacement magnitude vs. frequency, and the bottom graph shows acceleration magnitude vs. frequency. Two important characteristics that are common to virtually all of the sources measured are: (a) there is a large peak in magnitude somewhere below 200 Hz, which can be referred to as the fundamental mode, and (b) the acceleration spectrum is relatively flat with frequency, which means that the displacement spectrum falls of as $1/\omega^2$. These two characteristics are clearly visible in the plots shown in Fig. 2.

Table 2 characterizes many of the vibration sources measured in terms of the frequency and acceleration magnitude of the fundamental vibration mode. Information about the potential vibration sources is important to

the design of vibration converters for at least three reasons. First, the devices should be designed to resonate at the fundamental vibration frequency, which is quite low and may be difficult to obtain within 0.5 cm$^3$. Second, the higher frequency vibration modes are lower in acceleration magnitude than the low frequency fundamental mode. As will be explained in Section 4, the potential output power is proportional to $A^2/\omega$ where $\omega$ is the frequency of the fundamental vibration mode (and the natural frequency of the converter). Therefore, the design should target the low frequency fundamental mode. Third, in order to estimate the potential power generation, the magnitude and frequency of the driving vibrations must be known. Finally, it should be noted that the vibrations from the microwave oven, whose potential for energy conversion falls about in the middle of all the sources measured, have been used as a basis for

Table 2
Acceleration (m/s$^2$) magnitude and frequency of fundamental vibration mode for various sources

| Vibration source | $A$ (m/s$^2$) | $F_{peak}$ |
|---|---|---|
| Car engine compartment | 12 | 200 |
| Base of 3-axis machine tool | 10 | 70 |
| Blender casing | 6.4 | 121 |
| Clothes dryer | 3.5 | 121 |
| Person nervously tapping their heel | 3 | 1 |
| Car instrument panel | 3 | 13 |
| Door frame just after door closes | 3 | 125 |
| Small microwave oven | 2.5 | 121 |
| HVAC vents in office building | 0.2–1.5 | 60 |
| Windows next to a busy road | 0.7 | 100 |
| CD on notebook computer | 0.6 | 75 |
| Second story floor of busy office | 0.2 | 100 |

the simulations and testing of actual devices that will be presented later.

## 4. General model for vibration conversion

One can formulate a general model for the conversion of the kinetic energy of a vibrating mass to electrical power based on linear system theory without specifying the mechanism by which the conversion takes place. A simple model based on the schematic in Fig. 3 has been proposed by Williams and Yates [8]. This system is described by Eq. (1).

$$m\ddot{z} + (b_e + b_m)\dot{z} + kz = -m\ddot{y} \tag{1}$$

where $z$ is the spring deflection, $y$ the input displacement, $m$ the mass, $b_e$ the electrically induced damping coeff., $b_m$ the mechanical damping coeff. and $k$ is the spring constant.

The term $b_e$ represents an electrically induced damping coefficient. The primary idea behind this model is that the conversion of energy from the oscillating mass to electricity (whatever the mechanism is that does this) looks like a linear damper to the mass spring system. This is a fairly accurate model for certain types of electro-magnetic converters like the one analyzed by Williams and Yates [8]. For other types of converters (electrostatic and piezo-electric), this model must be changed somewhat. First, the effect of the electrical system on the mechanical system is not necessarily linear, and it is not necessarily proportional to velocity. Nevertheless, the conversion will always constitute a loss of mechanical kinetic energy, which can broadly be looked at as 'damping'. Even if this does not accurately model some types of converters, important conclusions can be made through its analysis, which can be extrapolated to electrostatic and piezoelectric systems.

The power converted to the electrical system is equal to the power removed from the mechanical system by $b_e$, the electrically induced damping. The electrically induced force is $b_e\dot{z}$. Power is the product of force and velocity, and therefore, the power converted is given by Eq. (2).

$$P = \frac{1}{2}b_e\dot{z}^2 \tag{2}$$
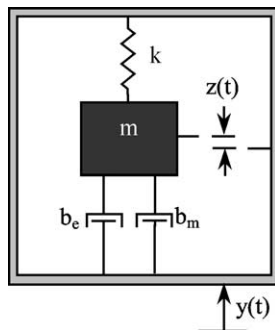
Eqs. (1) and (2) can be used to derive the following analytical expression for power converted.

$$|P| = \frac{m\zeta_e\omega_n\omega^2\left(\dfrac{\omega}{\omega_n}\right)^3 Y^2}{\left(2\zeta_T\dfrac{\omega}{\omega_n}\right) + \left(1 - \left(\dfrac{\omega}{\omega_n}\right)^2\right)^2} \tag{3}$$

where $|P|$ is the magnitude of output power, $Y$ the displacement magnitude of input vibrations, $\zeta_e$ the electrical damping ratio ($b_e = 2m\zeta_e\omega_n$), $\zeta_T$ the combined damping ratio ($\zeta_T = \zeta_e + \zeta_m$), $\omega$ the input frequency and $\omega_n$ is the natural frequency of spring mass sys.

If it is assumed that the resonant frequency of the spring mass system matches the input frequency, Eq. (3) can be reduced to the equivalent expressions in Eqs. (4) and (5).

$$|P| = \frac{m\zeta_e\omega^3 Y^2}{4\zeta_T^2} \tag{4}$$

$$|P| = \frac{m\zeta_e A^2}{4\omega\zeta_T^2} \tag{5}$$

where $A$ is the acceleration magnitude of input vibrations.

Note in Eq. (5) that the power is inversely proportional to frequency. Therefore, if the acceleration magnitude of the vibrations is constant or decreasing with frequency (as was shown to be the case in Section 3), then the converter should be designed to resonate at the lowest fundamental frequency in the input spectrum. Also note that power is optimized for $\zeta_m$ as low as possible, and $\zeta_e$ equal to $\zeta_m$. Because $\zeta_e$ is generally a function of circuit parameters, one can design in the appropriate $\zeta_e$ if $\zeta_m$ for the device is known. Finally, power is linearly proportional to mass. Therefore, the converter should have the largest proof mass that is possible while staying within the space constraints. An interesting tradeoff would occur if the space constraints did not allow enough mass for the converter to resonate at the lowest fundamental frequency. One may then want to target a higher frequency vibration mode. In practice, however, the authors have always been able to meet the lowest fundamental frequency within the given space constraints.

Fig. 4 shows the results of simulations based on this general model. The input vibrations were based on the measured vibrations from a microwave oven as described above, and the mass was limited by the requirement that the entire system stay within $1\,cm^3$. These same conditions were used for all simulations and tests throughout this paper; therefore all power output values can be taken to be normalized as power per cubic centimeter. Fig. 4 shows power out vs. electrical and mechanical damping ratio. Note that the values plotted are the logarithm of the actual simulated values The figure shows that for a given value $\zeta_m$,



Fig. 3. Schematic of generic vibration converter.
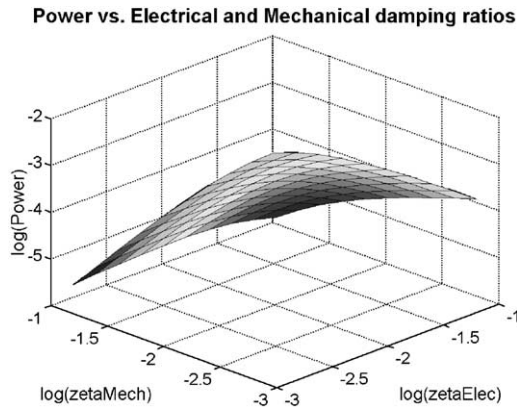
Fig. 4. Simulated output power vs. mechanical and electrical damping ratios. The logarithm of the actual values are plotted.

power is maximized for $\zeta_e = \zeta_m$. However, while there is a large penalty for the case where $\zeta_m$ is greater than $\zeta_e$, there is only a small penalty for $\zeta_e$ greater than $\zeta_m$. Therefore, a highly damped system will only slightly underperform a lightly damped system provided that most of the damping is electrically induced (attributable to $\zeta_e$).

## 5. Conversion mechanisms

There are three basic mechanisms by which vibrations can be converted to electrical energy: electro-magnetic, electrostatic, and piezoelectric. In the first case, the relative motion between a coil and a magnetic field causes a current to flow in the coil. Electrostatic generation consists of two conductors separated by a dielectric (i.e. a capacitor), which move relative to one another. As the conductors move the energy stored in the capacitor changes, thus providing the mechanism for mechanical to electrical energy conversion. Finally, mechanical strain in a piezoelectric material causes a charge separation across the material (which is a dielectric), producing a voltage.

Table 3 gives a qualitative comparison of the merits of each conversion mechanism. Electromagnetic converters have been demonstrated by Williams and Yates [8], and Amirtharajah and Chandrakasan [9]. The device built

Table 3
Comparison of the relative merits of three primary types of converters

| Mechanism | Advantages | Disadvantages |
|---|---|---|
| Piezoelectric | No voltage source needed Output voltage is 3–8 V | More difficult to integrate in microsystems |
| Electrostatic | Easier to integrate in microsystems | Separate voltage source needed Practical difficulties |
| Electro-magnetic | No voltage source needed | Output voltage is 0.1–0.2 V |

by Amirtharajah is about 2 cm in diameter and 7.5 cm in height. This generator produced a maximum output voltage of 180 mV. A 10–1 transformer was used to increase the voltage to the point where it could be rectified. Shearwood and Yates report only output power and not output voltage. However, the vibrations that they used to drive their device are far more energetic than those under consideration for this study. The voltage on the coil is determined by Faraday's Law. For simple geometries, it can be easily shown that for the vibration inputs under consideration in this study, an output voltage of only about 100 mV is possible within a volume of 1 cm$^3$. This would therefore necessitate a transformer, which would further increase the system size. Since there is no inherent advantage in using electro-magnetic converters over piezoelectric converters, it was determined to examine only piezoelectric and electrostatic converters in further detail.

The primary disadvantage of electrostatic converters is that they require a separate voltage source to initiate the conversion process. There are also some practical difficulties with their implementation that will be discussed later. The great advantage of electrostatic converters is that MEMS processing technology offers an effective method to obtain close integration with electronics. Additionally, the potential to scale down to much smaller sizes is greater for electrostatic converters. Piezoelectric converters do not require a separate voltage source, but they are not as easily integrated into a microfabrication process. While it is true that piezoelectric thin films can be integrated into MEMS processing [10], the piezoelectric coupling is greatly reduced. The design of both electrostatic (capacitive) converters and piezoelectric converters will be discussed in greater detail.

## 6. Electrostatic converters

The basis of electrostatic energy conversion is the variable capacitor. If the charge on the capacitor is constrained, the voltage will increase as the capacitance decreases. If the voltage across the capacitor is constrained, charge will move from the capacitor as the capacitance decreases. In either case, mechanical kinetic energy is converted to electrical energy. Meninger et al. [11] give a good explanation of the merits of charge constrained conversion vs. voltage constrained conversion. This project will work with charge constrained converters because two separate voltage sources are needed for voltage constrained conversion.

Because the primary advantage of electrostatic converters is their potential for integration in microsystems, silicon micromachining will be assumed as the fabrication process. Maximum capacitance is a critical
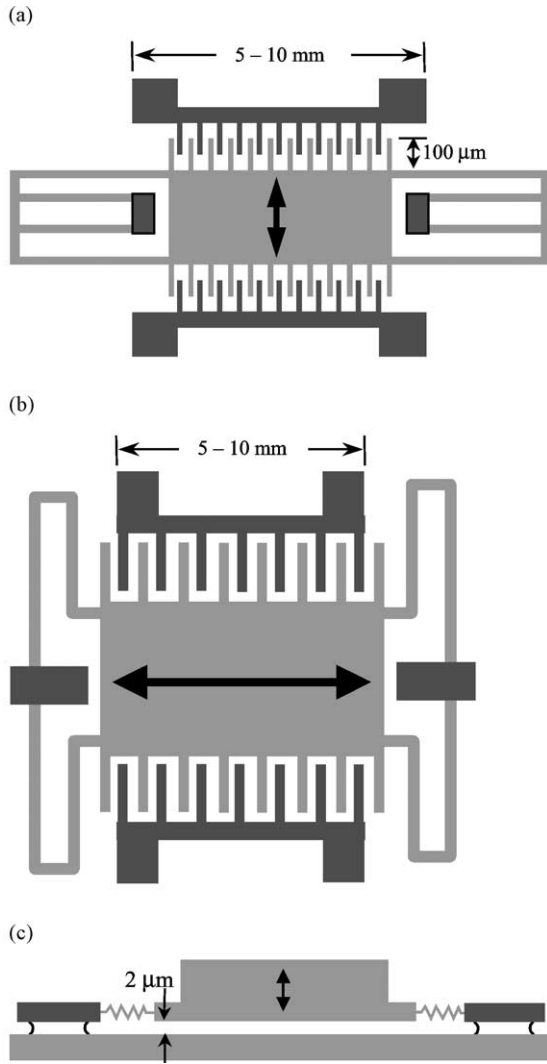
Fig. 5. Three types of electrostatic generators. (a) In-plane overlap converter: capacitance changes by changing overlap area of fingers (Not to scale). (b) In-plane gap closing converter: capacitance changes by changing gap between fingers (Not to scale). (c) Out-of-plane gap closing converter: capacitance changes by changing gap between two large plates (Not to scale).

parameter for electrostatic converters. Therefore, a deep reactive ion etching (DRIE) process capable of producing very thick, high aspect ratio features in silicon will be targeted [12]. The structures will be patterned in the top layer of a silicon on insulator (SOI) wafer, and a timed etch of the buried oxide will free the structures. Unetched oxide under silicon pads will serve as the anchors.

Three basic topologies for micromachined variable capacitors are shown in Fig. 5. The dark areas are fixed by anchors to the substrate, while the light areas are released structures that are free to move. The device shown in Fig. 5(a) will be referred to as an in-plane overlap converter because the change in capacitance arises from the changing overlap area of the many

Table 4
Comparison of three basic types of electrostatic converters

| Type | Advantages | Disadvantages |
|---|---|---|
| In-plane overlap | No mech. stops needed | Stability problems for large deflections |
| | Highest $Q$ factor | Lowest maximum capacitance |
| In-plane gap closing | Larger max. capacitance | Mechanical stops needed |
| Out-of-plane gap closing | Good stability | Largest mechanical damping |
| | Largest max capacitance | Surface adhesion |

interdigitated fingers. As the center plate moves in the direction shown, the overlap area, and thus the capacitance, of the fingers changes. Fig. 5(b) will be referred to as an in-plane gap closing converter because the capacitance changes due to the changing dielectric gap between the fingers. The device in shown in Fig. 5(c) will be referred to as an out-of-plane gap closing converter. Note that the figure shows a top view of the first two devices, and a side view of the third device. This third device oscillates out of the plane of the wafer, and changes its capacitance by changing the dielectric distance between two large plates. Table 4 provides a quick comparison of these three different types of converters. While the out-of-plane gap closing converter has the highest potential maximum capacitance, it has two major drawbacks. First, it has the most mechanical damping due to the large squeeze film damping forces between the two large plates. Second, the surface interaction between the two large plates will tend to make them stick together. Therefore, the minimum distance between the two plates (which determines the maximum capacitance) would likely be too great to make this design practical. The first problem may be solved by vacuum packaging the device, however, the second problem still makes this design impractical.

The dynamics of both in-plane overlap and gap closing converters can be described by the modified form of Eq. (1) given in Eq. (6). The exact form of $b_e(z)$ and $b_m(z,\dot{z})$ depends on the specifics of the implementation. Table 5 shows a general form of both damping terms for each type of converter.

$$m\ddot{z} + b_e(z) + b_m(z,\dot{z}) + kz = -m\ddot{y} \qquad (6)$$

Table 5
Damping terms for electrostatic converters

| Gap closing | Overlap |
|---|---|
| $b_e = \dfrac{q^2}{4N_g\varepsilon_0 tl}z$ | $b_e = \dfrac{q^2 d}{2N_g\varepsilon_0 t}\dfrac{1}{z^2}$ |
| $b_m = \dfrac{16N_g\mu t^3 l}{z^3}\dot{z}$ | $b_m = \left(\dfrac{N_g\mu tl}{d} + \dfrac{\mu A}{h}\right)\dot{z}$ |
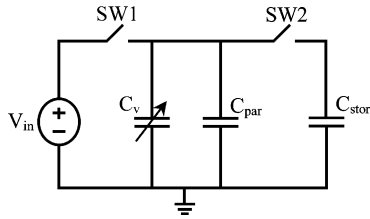
Fig. 6. Simple circuit representation for an electrostatic converter.

where $q$ is the charge on variable capacitor, $\varepsilon_0$ is the dielectric constant of free space, $\mu$ the viscosity, $t$ the device thickness, $l$ the finger length, $N_g$ the number of gaps between fingers, $d$ the distance between fingers, $h$ the distance between device layer and handle wafer and $A$ is the area of large center plate.

Using the simple charge pump circuit shown in Fig. 6, the energy output per cycle can be expressed by Eqs. 7(a) and 7(b).

$$E = \frac{1}{2} V_{in}^2 (C_{max} - C_{min}) \left( \frac{C_{max} + C_{par}}{C_{min} + C_{par}} \right) \qquad 7(a)$$

$$E = \frac{1}{2} V_{max} V_{in} (C_{max} - C_{min}) \qquad 7(b)$$

where $C_{max}$ is the maximum capacitance of variable capacitor $C_v$, $C_{min}$ the minimum capacitance of variable capacitor $C_v$, $C_{par}$ the parasitic capacitance, $V_{max}$ the max. voltage on variable capacitor $C_v$ and $V_{in}$ is the input, or charging, voltage

The second form of Eqs. 7(a) and 7(b) is useful to examine because it shows that the power output is limited by the maximum allowable voltage. The maximum voltage will be determined by the implementation of the switches, and if MOSFETS or diodes are used, it will likely be around 30 V. It is also useful to note that maximum voltage is determined by the relationship given in Eq. (8).

$$\frac{V_{max}}{V_{in}} = \frac{C_{max} + C_{par}}{C_{min} + C_{par}} \qquad (8)$$

Eqs. (6), (7a) and (7b) can be used to obtain approximate output power estimates for in-plane overlap and gap closing type converters. These estimates are graphed against the quality factor ($Q$) in Fig. 7. The quality factor may be defined as the magnitude of the transfer function at $\omega = \omega_n$ divided by its magnitude at $\omega = 0$. In this case, the transfer function, $H(j\omega)$, is derived from Eq. (6) and relates the spring deflection ($Z$) to the displacement magnitude of the input vibrations ($Y$). For a second order linear system, as described in Section 4, the value of $Q$ is $1/2\zeta$. The value of $Q$ is limited by both the mechanical and electrically induced damping. The maximum and minimum capacitances for the in-plane overlap converter are about 270 and 0.1 pF, respectively, for a $Q$ of 25. $C_{max}$ and $C_{min}$ for the in-plane gap closing converter are about 800 and 20 pF, respectively, at the optimal $Q$ (between 3.5 and 5 depending on the value of $C_{par}$).

It should be noted that for the in-plane gap closing converter, the number of fingers is related to $Q$. A higher $Q$
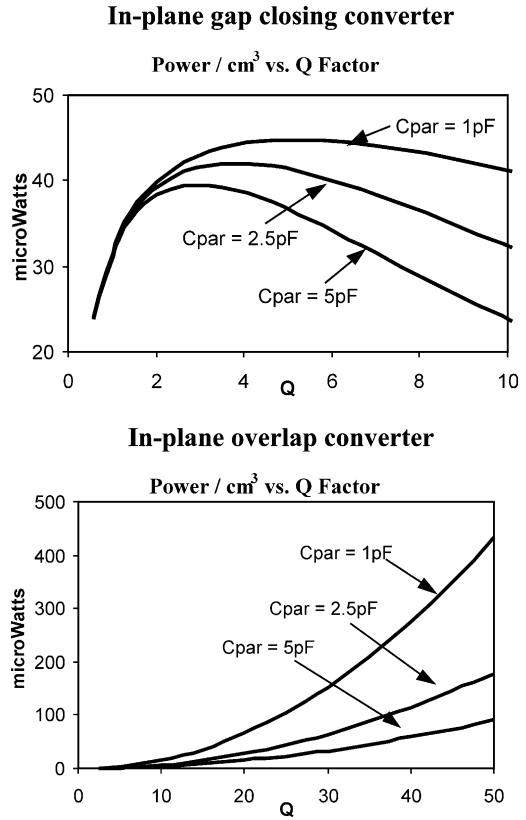


Fig. 7. Power vs. $Q$ factor for in-plane gap closing and overlap converters.

implies larger displacements. Since the fingers must be spaced far enough apart to accommodate this displacement, fewer fingers per unit length can be put on the structure. Therefore a higher $Q$ results in a lower maximum capacitance for in-plane gap closing converters. This is not true for in-plane overlap converters. The result is that for in-plane overlap converters, the higher the $Q$ factor, the more power output. However, there is an optimal $Q$ value (implying an optimal travel distance for the converter) for in-plane gap closing converters. Remembering the discussion of Section 4, the in-plane overlap converters should be capable of higher output power since their overall damping is lower. Fig. 7 verifies this observation. The curves in Fig. 7 are not the results of a complete design optimization, and as such are not meant to show the optimal power output for a given design topology, but rather to illustrate the relationship of output power on the travel distance. In particular, no limit was placed on the maximum voltage ($V_{max}$) for these power estimates.

Although the overlap converters are capable of higher power density, there are some very significant advantages to the gap closing converters. First, the maximum voltage developed across the capacitor is significantly lower because of a larger $C_{min}$. The maximum allowable voltage across the variable capacitor can be a very restrictive constraint, and it would most likely be impossible to design a high $Q$ converter with low parasitic capacitance and still stay below a reasonable maximum voltage across the variable capacitor. For example, an in-plane overlap

converter with a parasitic capacitance of 2.5 pF operating at a $Q$ factor of 25 would produce about 42 μW, but would generate a maximum voltage of about 100 V. An in-plane gap closing converter with the same parasitic capacitance and power output would only generate a maximum voltage of about 30 V. Second, the design of gap closing converters results in smaller spring deflections, which improves the stability of the system.

The potential stability problem with overlap type converters is demonstrated in Fig. 8. In the neutral position the oscillating structure is not very sensitive to a moment about its center of mass. (This moment could be induced by out of axis vibrations). However, when the flexures are extended to their maximum deflection, which would be on the order of 100 μm, the system is far more sensitive, or less stiff, to out of axis vibrations. Since the gap between fingers would be on the order of one to a few microns, it would only take a very small angular deflection to short the two electrodes of the capacitor, as shown in Fig. 8. Finally, the gap closing converter is a little less sensitive to the parasitic capacitance. For these reasons, it was decided that the in-plane gap closing converter represents the best alternative for electrostatic generators.

With the basic topology of the converter decided, a more detailed design optimization can be done. There are certain physical constraints that limit the design space. First, the total volume of the device must be less the 0.5 cm$^3$. This will limit the total system mass. It should be noted that additional mass will be added to the large oscillating silicon plate. Referring back to Eq. (5), the output power is linearly related to mass. The simulations shown below assume that this extra mass is made of tungsten, a very dense material.

**Converter in neutral position**

**Converter in extended position**
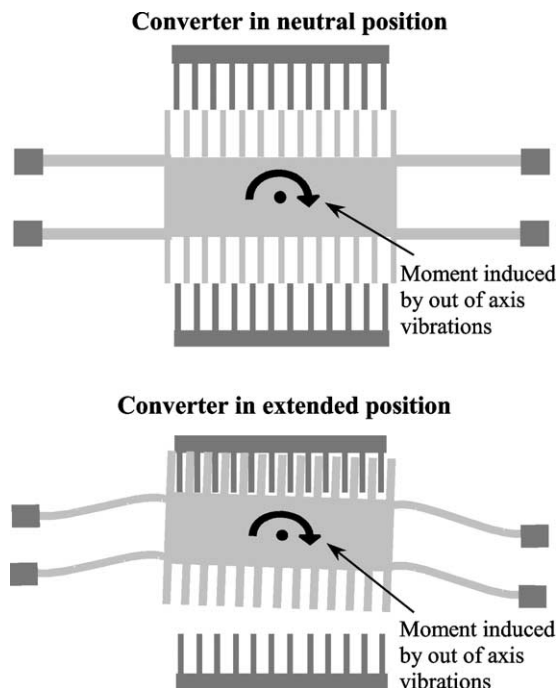
Fig. 8. Illustration of stability problem with in-plane overlap design.
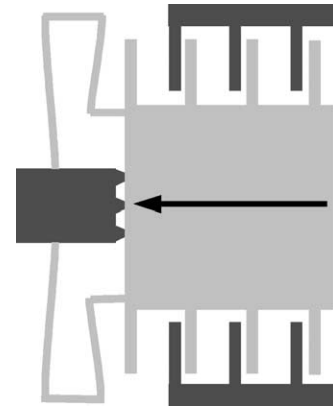


Fig. 9. Illustration of mechanical stops for in-plane gap closing converter.

As the proposed device is large compared to most MEMS structures, there are many methods in which the added mass could be incorporated. A second constraint is the maximum aspect ratio of features. The silicon DRIE process for which this converter is designed has a maximum aspect ratio of about 25. Third, if the fingers get two close, they will tend to stick, or pull in. Finally, perhaps the most restrictive constraint is the maximum allowable voltage. The voltage across $C_v$ can become very large. A maximum allowable voltage of 30 V has been used for simulations presented in this paper. This value is based on the limitations of MOS switches.

The following design parameters can be optimized: the input voltage ($V_{in}$), total length and width of the device, device thickness, finger length, and nominal gap between fingers. The maximum allowable voltage is closely related to the nominal gap between fingers. Note also that the system mass will be determined by the combination of the total volume constraint and the finger length. It should also be noted that physical stops need to be designed so that the fingers never make contact. This is illustrated in Fig. 9. The physical stops should be designed such that the when the mass collides with the stops, the fingers are at their minimum gap distance. This of course adds a collision, which will adversely affect the system dynamics, and could potentially remove a significant amount of kinetic energy. It has been shown that the coefficient of restitution for polysilicon micromechanical structures is about 0.5 [13]. The same study also showed no wear after $2.9 \times 10^9$ impacts, which would correspond to approximately one year of continuous operation at 100 Hz.

A formal optimization was performed in Matlab to determine the optimal design parameters. The optimal design parameters and output power are summarized in Table 6. The objective function for the optimization is the output power determined by a dynamic simulation of the system using Eqs. (6), (7a) and (7b). The optimal power output is 42.7 μW.

Fig. 10 shows the output power vs. device thickness and nominal gap between fingers. Other design parameters are as specified in Table 5. The lower right (high thickness and

Table 6
Optimal design parameters and power output for an in plane gap closing design

| Vars | Description | Value |
|------|-------------|-------|
| $w$ | Width of shuttle mass | 8.9 mm |
| $L$ | Length of shuttle mass | 6.7 mm |
| $L_{fin}$ | Length of fingers | 3.0 mm |
| $t$ | Device thickness | 202 μm |
| $V_{in}$ | Input voltage | 3.7 V |
| Gap | Nominal gap between fingers | 10 μm |
| Pout | Output power | 42.7 μW |

low nominal gap) is missing because that portion of the design space is not feasible with a maximum aspect ratio of 25. The darkened portion of the response surface violates the constraint that the maximum voltage across the variable capacitor be below 30 V. The figure clearly illustrates that relaxing the maximum voltage constraint results in significantly higher power output. It also shows that power output is highly dependent on device thickness, which should only be limited by the maximum allowable voltage. Finally, the optimal nominal gap is relatively small. (Note that the input vibrations for this system are about 5 μm in amplitude). This indicates, as mentioned previously, that there is an optimal quality factor ($Q$), and that the optimal $Q$ is very low resulting in a highly damped system.

## 7. Piezoelectric converters

When a piezoelectric material is placed under a mechanical stress, an open circuit voltage (a charge separation) appears across the material. Likewise, if a voltage is put across the material, a mechanical stress (and/or strain depending on how the material is constrained) develops in the material. The constitutive equations for piezoelectric material, which describe the mechanical and

**Output Power vs. Device Thickness and Nominal Gap**
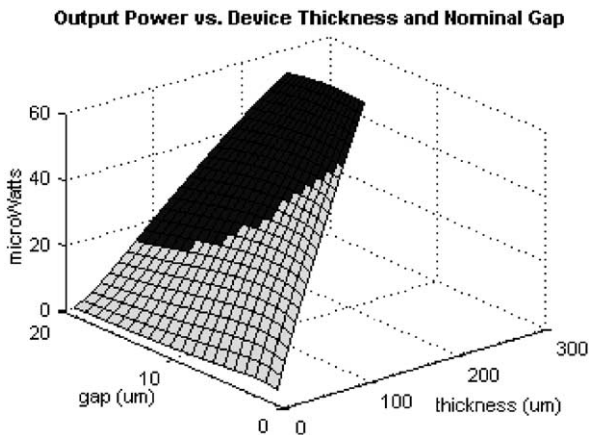
Fig. 10. Output power as a function of device thickness and nominal gap. The darkened section of the surface violates the 30 V maximum voltage constraint.
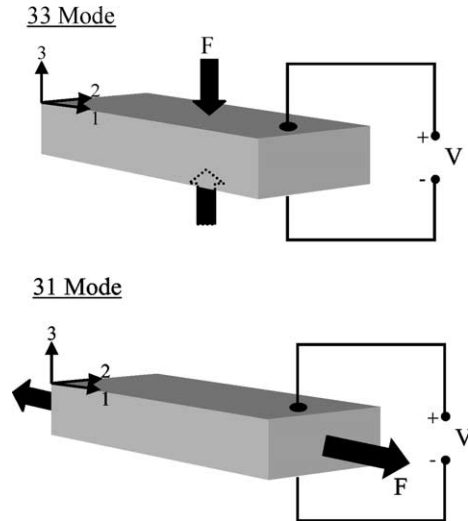
Fig. 11. Illustration of 33 mode and 31 mode operation for piezoelectric material.

electrical behavior, are given in Eqs. (9) and (10).

$$\delta = \sigma/Y + dE \tag{9}$$

$$D = \varepsilon E + d\sigma \tag{10}$$

where $\delta$ is the mechanical strain, $\sigma$ the mechanical stress, $Y$ the modulus of elasticity (Young's modulus), $D$ the electrical displacement (charge density), $E$ the electric field, $\varepsilon$ the dielectric constant, $d$ is the piezoelectric strain coefficient.

If the piezoelectric coupling term ($d$) is left out, these equations are just the uncoupled equations for an elastic dielectric material. The mechanical-to-electrical coupling provides the mechanism for power generation from vibrations.

Fig. 11 illustrates two different modes in which piezoelectric material may be used. The $x$, $y$, and $z$ axes are labeled 1, 2, and 3. Typically, piezoelectric material is used in the 33 mode, meaning that both the voltage and stress act in the 3 direction. However, the material can also be operated in the 31 mode, meaning that the voltage acts in the 3 direction (i.e. the material is poled in the 3 direction), and the mechanical stress acts in the 1 direction. Operation in 31 mode leads to the use of thin bending elements in which a large strain in the 1 direction is developed due to bending. The most common type of 31 elements are bimorphs, in which two separate sheets are bonded together, sometimes with a center shim in between them. Bimorphs can be poled such that the voltage across the two layers adds (series operation), or such that the charge adds (parallel operation). Fig. 12 illustrates the operation of piezoelectric bimorphs.

Although the electrical/mechanical coupling for 31 mode is lower than for 33 mode, there is a key advantage to operating in 31 mode. The system is much more compliant, therefore larger strains can be produced with smaller input forces. Also, the resonant frequency is much lower. An immense mass would be
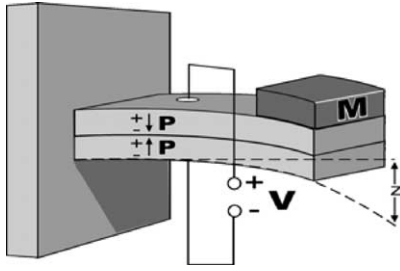
Fig. 12. Operation of a piezoelectric bimorph.

required in order to design a piezoelectric converter operating in 33 mode with a resonant frequency somewhere around 120 Hz. Therefore, the use of bending elements operating in 31 mode is essential in this case.

A bending element could be mounted in many ways to produce a generator. A cantilever beam configuration with a mass placed on the free end (see Fig. 12) has been chosen for two reasons. First, the cantilever mounting results in the lowest stiffness for a given size, and even with the use of bending elements it is difficult to design for operation at about 120 Hz in less than 0.5 cm³. Second, the cantilever configuration results in a relatively high average strain for a given force input.

Assuming this basic configuration, an analytic model can be developed based on beam theory and Eqs. (9) and (10). For the purposes of this model, it is assumed that the output from the piezoelectric bender is simply terminated with a resistive load, which results in the equivalent circuit shown in Fig. 13. The piezoelectric element is modeled as an AC voltage in series with a capacitor [14]. The resulting system model is given Eqs. (11) and (12).

$$\ddot{\delta} = \frac{-k_{\mathrm{sp}}}{mk}\delta - \frac{b_{\mathrm{m}}}{m}\dot{\delta} + \frac{k_{\mathrm{sp}}d}{mt}V_{\mathrm{R}} + \frac{3b}{2l^2}\ddot{y} \quad (11)$$

$$\dot{V}_{\mathrm{R}} = \frac{-Ydg}{k\varepsilon}\dot{\delta} - \frac{1}{RC}V_{\mathrm{R}} \quad (12)$$

where

$$k_{\mathrm{sp}} = \frac{3YI}{l^3}$$

$$k = 1 - \frac{Yd^2}{\varepsilon} = 1 - k_{31}^2$$

$k_{31}$ is the piezoelectric coupling coefficient, $V_{\mathrm{R}}$ the voltage across load resistance, $C$ the capacitance of piezoelectric

Piezoelectric Generator
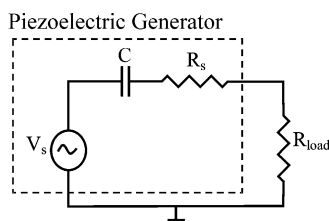


Fig. 13. Equivalent circuit for a piezoelectric generator.

element, $R$ the load resistance, $I$ the moment of inertia of beam, $t$ the thickness of piezoelectric material and $y$ is the displacement of input vibrations.

Assuming that the frequency of input vibrations ($\omega$) is equal to the undamped natural frequency of the device ($\omega_{\mathrm{n}}$), Eqs. (11) and (12) can be used to derive the analytic expression for power output given in Eq. (13), and the expression for the optimal load resistance given in Eq. (14).

$$|P| = \frac{RC^2\left(\frac{Ydg}{k\varepsilon}\right)^2}{(2\zeta\omega^2RC)^2 + (\omega^2RC(1-k) + 2\zeta\omega)^2}\frac{3b}{2l^2}|A|^2 \quad (13)$$

$$R_{\mathrm{opt}} = \frac{1}{\omega C}\frac{2\zeta}{\sqrt{4\zeta^2 + k_{31}^4}} \quad (14)$$

where $A$ is the acceleration magnitude of input vibrations.

If there were no piezoelectric coupling (i.e. the coupling coefficient $k_{31} = 0$), the optimal load resistance would just be $1/\omega C$, which is obvious by inspection of the circuit in Fig. 13.

This model is similar in many respects to the general second order model given in Eq. (1). Although this model is third order, it is linear, and Eq. (11) is in the same basic form as Eq. (1). The electrical coupling term, $(k_{\mathrm{sp}}d/mt)V_{\mathrm{R}}$, in Eq. (11) can be used to find the equivalent linear damping ratio, $\zeta_{\mathrm{e}}$, given in Eq. (15).

$$\zeta_{\mathrm{e}} = \frac{\omega k_{31}^2}{\sqrt{\omega^2 + 1/(RC)^2}} \quad (15)$$

Note, that by proper selection of the load resistance ($R_{\mathrm{opt}}$ given in Eq. (14)), $\zeta_{\mathrm{e}}$ will be equal to the mechanical damping ratio $\zeta$.

As in the case of the electrostatic generator design, with the basic topology decided, a formal optimization can be performed in order to choose parameter values. The parameters over which the design is optimized, and the design constraints are shown in Table 7. Designs with two common piezoelectric materials have been considered: lead zirconate titanate (PZT), which is a ceramic, and polyvinylidene fluoride (PVDF), which is a polymer. As in the design of the electrostatic generator presented in Section 6, the simulated output power was used as the 'objective

Table 7
Optimization variables and constraints

| Vars | Description | Constraints |
|---|---|---|
| $l_{\mathrm{m}}$ | Mass length | $h_{\mathrm{m}} < 5$ mm |
| $h_{\mathrm{m}}$ | Mass height | $(l_{\mathrm{m}} + l_{\mathrm{b}})w_{\mathrm{m}} < 1$ cm² |
| $w_{\mathrm{m}}$ | Mass width | $(l_{\mathrm{m}} + l_{\mathrm{b}})w_{\mathrm{b}} < 1$ cm² |
| $l_{\mathrm{b}}$ | Beam length | $l_{\mathrm{e}} - l_{\mathrm{m}} < 0$ |
| $w_{\mathrm{b}}$ | Beam width | $\delta_{\max} < \delta_{\mathrm{yield}}$ |
| $l_{\mathrm{e}}$ | Electrode length | $\omega_{\mathrm{n}} \approx 2\pi \times 120$ |
| $t_{\mathrm{p}}$ | Piezo layer thickness | |
| $t_{\mathrm{sh}}$ | Steel shim thickness | |
| $R_{\mathrm{load}}$ | Load resistance | |

Table 8
Optimal design parameters for two different materials with and without a center shim

|  | PZT | | PVDF | |
| --- | --- | --- | --- | --- |
|  | No shim | Shim | No shim | Shim |
| $l_m$ (cm) | 1.71 | 1.73 | 0.32 | 0.5 |
| $h_m$ (cm) | 0.5 | 0.5 | 0.5 | 0.5 |
| $w_m$ (cm) | 0.3 | 0.3 | 1.87 | 1.32 |
| $l_b$ (cm) | 1.62 | 1.6 | 0.21 | 0.25 |
| $w_b$ (cm) | 0.3 | 0.3 | 1.87 | 1.32 |
| $l_e$ (cm) | 1.62 | 1.6 | 0.21 | 0.25 |
| $t_p$ (μm) | 365 | 267 | 75.6 | 42.9 |
| $t_{sh}$ (μm) | 0 | 182 | 0 | 135 |
| $R_{load}$ (kΩ) | 355 | 262.5 | 6725 | 4825 |
| $V_r$ (v) | 13.1 | 12.1 | 50 | 50 |
| $P_{out}$ (μW) | 242 | 277 | 186 | 260 |

function' for the optimization. The resulting parameter and output power values for both PZT and PVDF bimorphs are shown in Table 8. The vibration input was again based on that measured on a small microwave oven, which has an input magnitude of 2.5 m/s$^2$ at approximately 120 Hz. The piezoelectric coupling coefficient ($k_{31}$) for PZT used in the simulation was 0.12 based on measurements taken on a PZT bimorph with a steel center shim. The coupling coefficient used for PVDF was 0.08 based on published data [4,14]. Finally, a mechanical damping ratio of 0.01 was used based on measurements.

An additional constraint was added on the maximum output voltage (50 V) for the PVDF simulations. Although 50 V is quite high, this could be reduced by using thinner multi-layer laminates rather than a single layer for each side of the bimorph. Using multi-layer laminates would also significantly decrease the optimal load resistance. Notice that the optimal design parameters for the PZT bimorphs result in a very long thin device. Depending on the application, additional individual constraints could be put on the total length or width of the device, rather than just on the total area. Referring to Table 7, the best obtainable output power is about 250 μW. This matches the power
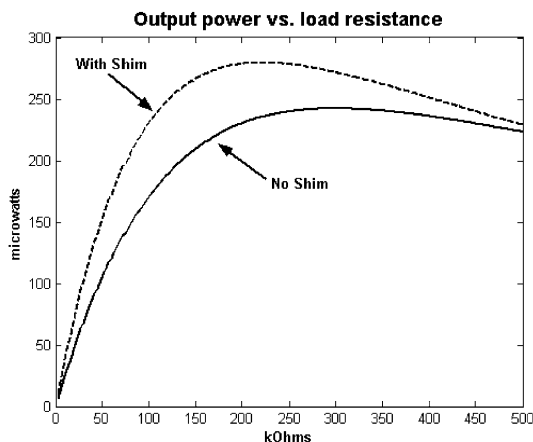


Fig. 14. Simulated output power vs. load.
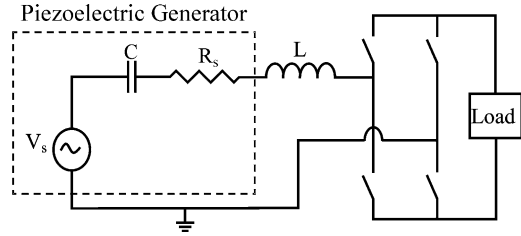


Fig. 15. Piezoelectric converter with series inductor and active bridge circuit.

predicted by the general model discussed in Section 4 very well, which results in an output power of 252 μW for the same input, damping conditions, and mass.

The simulated output power for the two PZT bimorphs, using optimal design parameters, vs. the load resistance is shown in Fig. 14. The effective electrical damping ratio, calculated from Eq. (15), at the optimal load resistance is 0.01, which matches the mechanical damping ratio used in the simulations. Note also that there is a large penalty if the load impedance is too low, but there is a much smaller penalty if it is too high. The effective electrical damping ratio increases as the load resistance increases. Therefore, the curves in Fig. 13 are consistent with the simulations using the general model of Section 4 shown in Fig. 4, which indicate that while the optimal point is at $\zeta_e = \zeta_m$, the penalty for increasing $\zeta_e$ is small. The power train circuitry should attempt to allow optimal power transfer from the load while still meeting the voltage and current requirements of the target system.

Looking at the circuit in Fig. 13, it is obvious that more efficient power transfer to the load could be obtained by inserting a series inductor to cancel the capacitive reactance. The value of this inductor would be $L = 1/\omega^2 C$. Given the very low frequencies at which this converter must operate, the resulting inductance is on the order of hundreds of Henrys, which is clearly too large to be practical. However, an active bridge circuit like the one shown in Fig. 15 could potentially be used with a smaller inductor and a clever control scheme to significantly increase the power transfer to the load. The design of this circuit and controller are beyond the scope of the current project. It is sufficient to note here that the output power of a piezoelectric generator could potentially be significantly increased.

## 8. Prototype testing and results

A bimorph made of PZT with a steel center shim was used as a prototype to verify the model in Eqs. (10) and (11). The bimorph, with attached mass and fixture, is shown in Fig. 16.

The total size of the bimorph and mass is approximately 1 cm$^3$. The measured and simulated output power vs. load resistance is plotted in Fig. 17. The converter was driven with vibrations at 100 Hz with an acceleration magnitude of 2.25 ms$^{-2}$. Again, these vibrations are roughly equivalent to
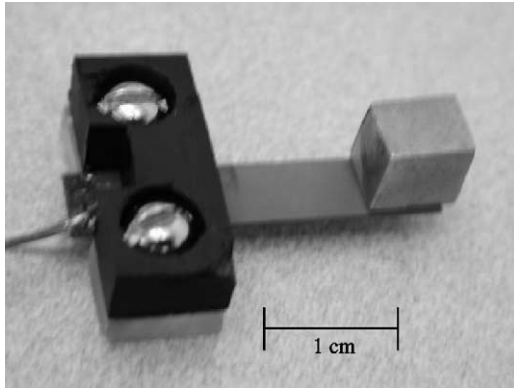
Fig. 16. PZT bender with mass and fixture.

those measured on a small microwave oven. The beam length and mass were chosen so that the system's natural frequency matched the driving frequency. The mechanical damping ratio, $\zeta$, was measured as 0.01, and the piezo-electric coupling coefficient, $k_{31}$, was measured to be 0.12. Other material properties were taken from published data [15]. The good agreement between experiments and simulations verifies that the model shown in Eqs. (10) and (11) is sufficiently accurate to use for design and optimization purposes. Furthermore, the optimal power output values shown in Section 7 should be obtainable.

The AC output voltage magnitude is also of importance. Fig. 18 shows the simulated and measured
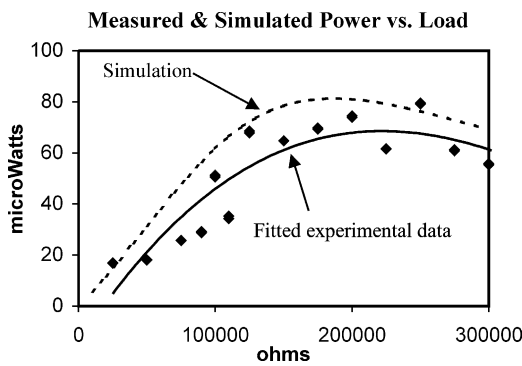


Fig. 17. Measured and simulated power out vs. load resistance.
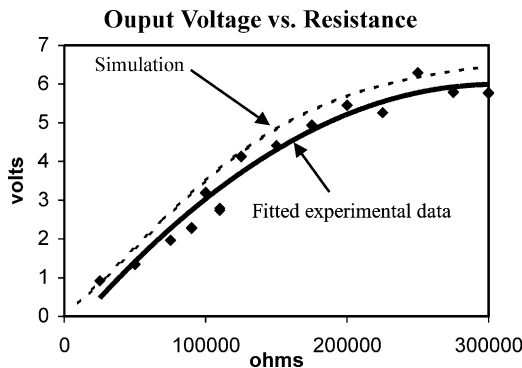


Fig. 18. Measured and simulated AC output voltage magnitude vs. load resistance.
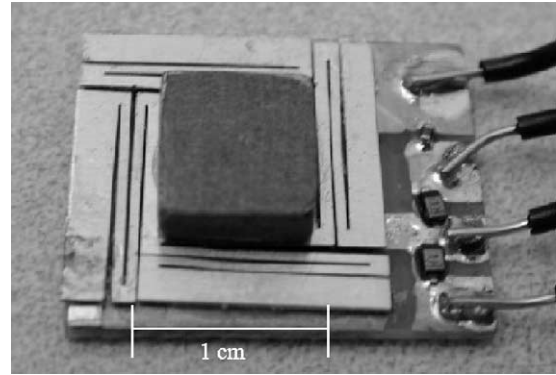


Fig. 19. Large scale capacitive prototype.

Table 9
Test data for large scale capacitive prototype

| $V_{source}$ | $C_{out}$ | $\Delta V_{out}$/cycle (V) | $E_{out}$/cycle (J) |
|---|---|---|---|
| 3 | $200 \times 10^{-12}$ | 0.25 | $6 \times 10^{-12}$ |
| 9 | $200 \times 10^{-12}$ | 1 | $1 \times 10^{-9}$ |

output voltage magnitude vs. load resistance. The bimorph used was poled for series operation. If a bimorph poled for parallel operation was used instead, the optimal load resistance would be cut by a factor of 4, the output voltage would be cut in half, and the output current would increase by a factor of 2. In either case, the output voltage is on the right order of magnitude.

A relatively large capacitive prototype has been fabricated and tested as a proof of concept. The total footprint area is about 3 cm$^2$. The prototype is shown in Fig. 19. This is an out-of-plane gap closing type converter. The purpose of the converter was to quickly verify that the concept and circuit shown in Fig. 6 is viable, rather than to build a device optimized for output power. Table 9 shows the essential testing data for this device.

Both in-plane overlap and gap closing converters have been designed and are in fabrication using the DRIE process previously mentioned. A closeup of the interdigitated fingers on a preliminary test device is shown in Fig. 20.
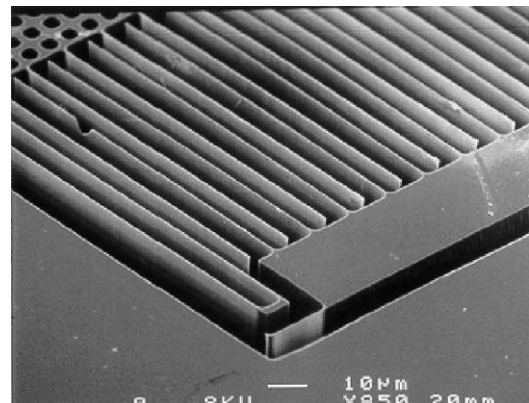


Fig. 20. Closeup of in-plane gap closing converter prototype.

This device was used to test fabrication and assembly methods and to test parasitic capacitances.

## 9. Conclusions and future work

1. Powering small wireless sensor nodes from ambient vibrations is viable and attractive for certain applications. The design of converters should take into consideration the fundamental characteristics of the vibration spectrum of the environment in which the converter will be used. Low level vibrations occurring on many household appliances and everyday objects in and around buildings appear to have a fundamental mode on the order of 100 Hz, and maximum acceleration magnitudes in the range of $0.5-5 \text{ ms}^{-2}$.

2. The analysis presented in this paper indicates that piezoelectric converters will be capable of converting more power per unit volume than capacitive converters. Piezoelectric converters are also favorable because they require no separate voltage source, and because the output voltage for the vibration sources under consideration is in the range of $3-10$ V. While capacitive converters require a separate voltage source, and are not capable of converting as much power per unit volume, they are still attractive because they offer more potential for integration with microsystems. Of the three types of capacitive converters discussed, the in-plane gap closing capacitor appears to be the most attractive design topology because of its robustness yet still high power conversion potential.

3. More work is now in process on designing very energy efficient, simple power electronics to rectify and regulate the power for use by electronics.

## References

[1] A. Chandrakasan, R. Amirtharajah, J. Goodman, W. Rabiner, Trends in low power digital signal processing, Proceedings of the 1998 IEEE International Symposium on Circuits and Systems (1998) 604–607.

[2] W.R. Davis, N. Zhang, K. Camera, F. Chen, D. Markovic, N. Chan, B. Nikolic, R.W. Brodersen, A design environment for high throughput, low power dedicated signal processing systems, Proceedings of the IEEE Custom Integrated Circuits Conference (2001) 545–548.

[3] M. Stordeur, I. Stark, Low power thermoelectric generator-self-sufficient energy supply for micro systems, 16th International Conference on Thermoelectrics (1997) 575–577.

[4] T. Starner, Human-powered wearable computing, IBM Systems Journal 35 (3) (1996) 618–629.

[5] N.S. Shenck, J.A. Paradiso, Energy scavenging with shoe-mounted piezoelectrics, IEEE Micro 21 (2001) 30–41.

[6] A. Mehra, X. Zhang, A.A. Ayon, I.A. Waitz, M.A. Schmidt, C.M. Spadaccini, A six-wafer combustion system for a silicon micro gas turbine engine, Journal of Microelectromechanical Systems 9 (4) (2000) 517–526.

[7] W.Y. Sim, G.Y. Kim, S.S. Yang, Fabrication of micro power source (MPS) using a micro direct methanol fuel cell (μDMFC) for the medical application, Technical Digest MEMS 2001 (2001) 341–344.

[8] C.B. Williams, R.B. Yates, Analysis of a micro-electric generator for microsystems, Proceedings of the Transducers 95/Eurosensors IX (1995) 369–372.

[9] R. Amirtharajah, A.P. Chandrakasan, Self-powered signal processing using vibration-based power generation, IEEE Journal of Solid-State Circuits 33 (1998) 687–695.

[10] S.S. Lee, R.M. White, Self-excited piezoelectric cantilever oscillators, Proceedings of the Transducers 95/Eurosensors IX (1995) 41–45.

[11] S. Meninger, J.O. Mur-Miranda, R. Amirtharajah, A.P. Chandrakasan, J.H. Lang, Vibration-to-electric energy conversion, IEEE Transactions on the VLSI System 9 (2001) 64–76.

[12] R. Yeh, S. Hollar, K.S.J. Pister, Single mask, large force, and large displacement electrostatic linear inchworm motors, Technical Digest MEMS 2001 (2001).

[13] A.P. Lee, A.P. Pisano, Repetitive impact testing of micromechanical structures, Sensors and Actuators A (Physical) A39 (1) (1993) 73–82.

[14] V.H. Schmidt, Theoretical electrical power output per unit volume of PVF2 and mechanical-to-electrical conversion efficiency as functions of frequency, Proceedings of the Sixth IEEE International Symposium on Applications of Ferroelectrics (1986) 538–542.

[15] Piezoelectric Actuator/Sensor Kit Manual, Piezo Systems Inc., Cambridge MA, 1998.

**Shad Roundy** is currently a graduate student in the Mechanical Engineering department at UC Berkeley. He works in the Integrated Manufacturing Lab under the advisement of Prof. Paul Wright. He received his BS in Mechanical Engineering from Brigham Young University in 1996. He was planning on coming to UC Berkeley to start graduate school in the fall of 1996, but decided at the last minute that some industry experience would be valuable before starting graduate school. So, he went to work for Hewlett Packard for two years. He worked as a manufacturing process development engineer in HP's Inkjet business. His primary responsibility was to oversee the process control effort for a particular assembly line, and later for a product development team. He also led a worldwide group of process control engineers coordinating the effort for two product lines. He also worked on the development of new assembly processes. After two years, he returned to school at UC Berkeley.His main project is to explore ways to 'scavenge' power for small wireless sensor nodes. Specifically, he is working on designing devices to convert low-level ambient vibrations to electricity for use by the wireless nodes.

**Paul Kenneth Wright** was born in London and obtained his degrees at the University of Birmingham, England. He is now the A. Martin Berlin Prof. of Mechanical Engineering at Berkeley. Within the College of Engineering, he is the co-chairman of the Management of Technology Program, and the Associate Dean for Distance Learning and Instructional Technology. He has written numerous articles for journals, conferences, and symposiums, as well as co-authored 'Manufacturing Intelligence', with D.A. Bourne, and 'Metal Cutting', with E.M. Trent. In addition, he serves as a consultant and is involved in many professional organizations. His most recent book '21st Century Manufacturing' just won the book of the year award from the Society of Manufacturing Engineers.

**Jan M. Rabaey** received the EE and PhD degrees in applied sciences from the Katholieke Universiteit Leuven, Belgium, respectively, in 1978 and 1983. From 1983 to 1985, he was connected to the University of California, Berkeley as a Visiting Research Engineer. From 1985 to 1987, he was a research manager at IMEC, Belgium, and in 1987, he joined the faculty of the Electrical Engineering and Computer Science department of the University of California, Berkeley, where he holds the Donald O. Pederson Distinguished Professorship. From 1999 to 2002, he has served as the associate chair of the EECS Department at Berkeley. He is the scientific co-director of the Berkeley Wireless Research Center (BWRC), and serves as director of the GigaScale Research Center (GSRC).He received numerous scientific awards, including the 1985 IEEE Transactions on Computer Aided Design Best Paper Award (Circuits and Systems Society), the 1989 Presidential Young Investigator award, and the 1994 Signal Processing Society Senior Award. He is an IEEE Fellow.His current research interests include the conception and implementation of next-generation integrated wireless systems. This includes the analysis and optimization of communication algorithms and networking protocols, the study of low-energy implementation architectures and circuits, and the supporting design automation environments.